

Response to the editor

We thank the editor for their valuable and helpful comments. Our responses to the comments are provided below in bold font with the editor's comments in italicized font.

Comments to the Author:

This paper looks good to go, however there are a couple of technical points raised by reviewer 2 that I do not feel have been adequately addressed and these need to be fixed before publication:

1. I'm afraid that I have to agree with the reviewer concerning the terminology of the impacts. Using the strict IPCC definitions, this work only deals with radiative impacts and while these will certainly have knock-on effects on climate, the two terms should not be conflated and as such, this work should not be presented as an evaluation of climate impacts. I would insist that terms like "the net global climate impacts" in the abstract (and elsewhere, e.g. lines 82, 458) are rephrased to "the net global radiative impacts". I would also change the title of section 3.4 to something like "Impacts of solid fuel cookstove aerosol emissions on radiative transfer"

Response: We agree with the editor. We have revised the term of “the net global climate impacts” in the text as “the net global radiative impacts” throughout the manuscript, e.g. (Page 1 Lines 26-29) “Without BC serving as ice nuclei (IN), global and Indian solid fuel cookstove aerosol emissions have a net global cooling radiative effects of $-141 \pm 4 \text{ mW m}^{-2}$ and $-12 \pm 4 \text{ mW m}^{-2}$, respectively (\pm represents modeled temporal standard deviations for $n=5$ run years).”

(Page 2 Lines 36-38) “When BC is allowed to behave as a source of IN, the net global radiative impacts of the global and Indian solid fuel cookstove emissions range from -275 to $+154 \text{ mW m}^{-2}$ and -33 to $+24 \text{ mW m}^{-2}$, with globally averaged values -59 ± 215 and $0.3 \pm 29 \text{ mW m}^{-2}$ respectively.”

(Page 3 Lines 82-84) “Bauer et al. (2010) estimated that the net global radiative impact of residential biofuel carbonaceous aerosol emissions is -130 mW m^{-2} .”

(Pages 15-16 Lines 442-445) “For the radiative impacts of global solid fuel cookstove emissions, global annual mean DRE is $+105 \pm 13 \text{ mW m}^{-2}$, which is $\sim 50\%$ higher than the default model scheme in which BC particles are not treated as IN (Fig. 6).”

We have also revised the title of Section 3.4 as (Page 11 Line 305) “3.4 Impacts of solid fuel cookstove aerosol emissions on global radiation budget”.

2. I thank the reviewers for addressing the point concerning uncertainty, but they failed to address one key technical query of the reviewer, which was to clarify whether the plus or minus uncertainty ranges represent standard deviations or some other measure. This is very important and should be stated, both in the main text and the abstract.

Response: We have added the description of uncertainty ranges in the abstract and main text as

(Page 1 Lines 24-29) “However, the model tends to underestimate AOD over India and China by $\sim 19 \pm 4\%$ but overestimate it over Africa by $\sim 25 \pm 11\%$ (\pm represents modeled temporal standard deviations for $n=5$ run years). Without BC serving as ice nuclei (IN), global and Indian solid fuel cookstove aerosol emissions have a net global cooling radiative effects of $-141 \pm 4 \text{ mW m}^{-2}$ and $-12 \pm 4 \text{ mW m}^{-2}$, respectively (\pm represents modeled temporal standard deviations for $n=5$ run years).”

(Page 8 Lines 236-238) “Over East Asia, the model slightly underestimates observed OA, with a NMB of $-8.5 \pm 5\%$ (\pm represents modeled temporal standard deviations for $n=5$ run years) (Fig. 2a).”

(Page 11 Lines 311-313) “For the global solid fuel cookstove sector, the globally averaged DRE from aerosol emissions is $+70 \pm 3 \text{ mW m}^{-2}$ (\pm represents modeled temporal standard deviations for $n=5$ run years) without treating BC as IN, which is a warming effect.”

(Page 13 Lines 373-376) “For the radiative effect of global solid fuel cookstove emissions with BC as IN, global annual mean DRE is $105 \pm 13 \text{ mW m}^{-2}$ (\pm represents standard deviations from modeling results with BC MFE values as 0.01, 0.05 and 0.1), ranging from $+90$ to $+115 \text{ mW m}^{-2}$, which is 29-64% higher than the DRE values from the default scheme (Fig. 6).”

Global radiative effects of solid fuel cookstove aerosol emissions

Yaoxian Huang^{1,a}, Nadine Unger², Trude Storelvmo³, Kandice Harper¹, Yiqi Zheng³, and Chris Heyes⁴

¹School of Forestry and Environmental Studies, Yale University, New Haven, CT 06511, USA

²College of Engineering, Mathematics and Physical Sciences, University of Exeter, Exeter, EX4 4QE, UK

³Department of Geology and Geophysics, Yale University, New Haven, CT 06511, USA

⁴International Institute for Applied Systems Analysis, Laxenburg, Austria

^anow at: Department of Climate and Space Sciences and Engineering, University of Michigan, Ann Arbor, MI 48109, USA

Correspondence to: Yaoxian Huang (yaoxian.huang1@gmail.com)

Abstract. We apply the NCAR CAM5-Chem global aerosol-climate model to quantify the net global radiative effects of black and organic carbon aerosols from global and Indian solid fuel cookstove emissions for the year 2010. Our assessment accounts for the direct radiative effects, changes to cloud albedo and lifetime (aerosol indirect effect, AIE), impacts on clouds via the vertical temperature profile (semi-direct effect, SDE), and changes in the surface albedo of snow and ice (surface albedo effect). In addition, we provide the first estimate of household solid fuel black carbon emission effects on ice clouds. Anthropogenic emissions are from the IIASA GAINS ECLIPSE V5a inventory. A global dataset of black carbon (BC) and organic aerosol (OA) measurements from surface sites and aerosol optical depth (AOD) from AERONET is used to evaluate the model skill. Compared with observations, the model successfully reproduces the spatial patterns of atmospheric BC and OA concentrations, and agrees with measurements to within a factor of 2. Globally, the simulated AOD agrees well with observations, with normalized mean bias close to zero. However, the model tends to underestimate AOD over India and China by $\sim 19 \pm 4\%$ but overestimate it over Africa by $\sim 25 \pm 11\%$ (\pm represents modeled temporal standard deviations, for $n=5$ run years). Without BC serving as ice nuclei (IN), global and Indian solid fuel cookstove aerosol emissions have a net global cooling radiative effects of $-141 \pm 4 \text{ mW m}^{-2}$ and $-12 \pm 4 \text{ mW m}^{-2}$, respectively (\pm represents modeled temporal standard deviations for $n=5$ run years). The net radiative impacts are dominated by the AIE and SDE mechanisms, which

Deleted: uncertainty range due to interannual internal climate model variability

Deleted: impact on global climate

originate from enhanced cloud condensation nuclei concentrations for the formation of liquid and mixed-phase clouds, and a suppression of convective transport of water vapor from the lower troposphere to the upper troposphere/lower stratosphere that in turn leads to reduced ice cloud formation. When BC is allowed to behave as a source of IN, the net global ~~radiative~~ impacts of the global and Indian solid fuel cookstove emissions range from -275 to +154 mW m⁻² and -33 to +24 mW m⁻², with globally averaged values -59 ± 215 and 0.3 ± 29 mW m⁻² respectively. Here, the uncertainty range is based on sensitivity simulations that alter the maximum freezing efficiency of BC across a plausible range: 0.01, 0.05 and 0.1. BC-ice cloud interactions lead to substantial increases in high cloud (< 500 hPa) fractions. Thus, the net sign of the impacts of carbonaceous aerosols from solid fuel cookstoves on global climate (warming or cooling) remains ambiguous until improved constraints on BC interactions with mixed-phase and ice clouds are available.

Deleted: climate

1. Introduction

Worldwide 2-3 billion people rely on solid fuels for the majority of their energy needs (Legros et al., 2009). This household biomass combustion includes burning wood fuel, agricultural residues and dung for cooking, heating and lighting. Emissions from household solid fuel combustion include greenhouse gases (carbon dioxide and methane), black carbon (BC), organic carbon (OC), and other trace gases (e.g., nitrogen oxides). Globally, BC from household solid fuel emissions accounts for approximately 25% of the total anthropogenic BC emissions (Bond et al., 2013). Among different types of cookstoves, advanced charcoal stoves show lowest BC emission factors, followed by simple charcoal, advanced biomass, rocket and simple wood stoves, respectively (Garland et al., 2017). India contains a large concentration of solid fuel-dependent households: approximately 160 million households use solid fuels for cooking (Venkataraman et al., 2010). In India, residential biofuel combustion represents the dominant energy sector and accounts for over 50% of the total source of BC and OC emissions (Klimont et al., 2009). India has a long history of unsuccessful stove intervention programs that have sometimes focused on health benefits (Hanbar and Karve, 2002; Kanagawa and Nakata, 2007; Kishore and Ramana, 2002). Despite years of interventions, the vast majority of Indian households still rely on traditional stoves (Legros et al., 2009). The possible scope for global climate co-benefits in future Indian cookstove intervention programs warrants further examination and analysis of this region. BC-rich household solid fuel emission plays an important role in affecting regional air quality (Archer-Nicholls et al.,

64 2016; Carter et al., 2016; Liu et al., 2016) and influencing global climate change (Bauer et al.,
65 2010; Butt et al., 2016; Venkataraman et al., 2005). The human health consequences of solid fuel
66 combustion are substantial (Archer-Nicholls et al., 2016; Ezzati and Kammen, 2002; Lelieveld et
67 al., 2015). Nearly 9% of the global burden of disease is attributable to exposure to household air
68 pollution from solid fuels, equivalent to 2.9 million premature deaths and 86 million disability
69 adjusted life years (DALYs) annually (GBD 2015 Risk Factors Collaborators, 2016). Half of the
70 world's population is exposed to indoor air pollution, mainly attributable to solid fuel usage for
71 household cooking and heating (Bonjour et al., 2013; Smith et al., 2014).

72 Carbonaceous aerosols from solid fuel combustion interact with the Earth's radiation budget
73 directly by absorbing and scattering solar radiation (direct radiative effect, DRE) and indirectly by
74 changing cloud albedo and lifetime (aerosol indirect effect, AIE), modifying the vertical
75 temperature profile (semi-direct effect, SDE), and changing the surface albedo over snow and ice
76 (surface albedo effect, SAE) (Boucher et al., 2013; Chung, 2005; Chylek and Wong, 1995; Ghan,
77 2013; Ghan et al., 2012; Myhre et al., 2013). Carbonaceous aerosols affect cloud albedo and
78 lifetimes (the AIE) by acting as cloud condensation nuclei (CCN) or ice nuclei (IN), thus
79 modifying cloud properties and changing the top-of-atmosphere (TOA) radiative fluxes
80 (Lohmann, 2002; Lohmann et al., 2000; Penner et al., 1992; Pierce et al., 2007; Spracklen et al.,
81 2011b). The net climatic effect of carbonaceous aerosols from household solid fuel combustion is
82 not well constrained and even the sign is uncertain (Bond et al., 2013). Bauer et al. (2010)
83 estimated that the net global radiative impact of residential biofuel carbonaceous aerosol emissions
84 is -130 mW m^{-2} . Kodros et al. (2015) have estimated that net DRE of solid fuel aerosol emissions
85 ranges from -20 to $+60 \text{ mW m}^{-2}$, AIE from -20 to $+10 \text{ mW m}^{-2}$, with uncertainties due to
86 assumptions of the aerosol emission masses, size distribution, aerosol optical properties and
87 mixing states. Butt et al. (2016) reported that the net DRE and AIE of aerosols from the residential
88 emission sector (including coal) ranged from -66 to $+21 \text{ mW m}^{-2}$, and from -52 to -16 mW m^{-2} ,
89 respectively. Their study did not include greenhouse gases. Moreover, neither of the latter two
90 studies consider the aerosol cloud-lifetime effect (second indirect effect), SDE and SAE. From the
91 perspective of policy-relevant country-level assessment of cookstove burning on global climate,
92 Lacey and Henze (2015) revealed that solid fuel cookstove aerosol emissions resulted in global air
93 surface temperature changes ranging from 0.28 K cooling to 0.16 K warming; Lacey et al. (2017)

Deleted: aerosol

Deleted: climate

96 further concluded that emissions reductions, including both aerosols and greenhouse gases, from
97 China, India and Ethiopia contributed the most to the global surface temperature changes by 2050.

98 None of the previous assessments have included BC-ice cloud interactions that can exert a large
99 influence on the atmospheric radiation balance. A recent study by Kulkarni et al. (2016) showed
100 that BC could act as IN, which was also shown by past lab and field findings (Cozic et al., 2008;
101 DeMott et al., 1999; Koehler et al., 2009). With BC as IN, Penner et al. (2009) estimated that the
102 total radiative forcing of anthropogenic and biomass BC emissions was -300 to -400 mW m⁻², with
103 IN parameterizations following Liu and Penner (2005) and Kärcher et al. (2006). Gettelman et al.
104 (2012) further concluded that AIE from BC emissions was -60 mW m⁻², with ice nucleation
105 parameterization following Barahona and Nenes (2009). Hence, a re-assessment of the global
106 climate change impacts of carbonaceous aerosol emissions from the solid fuel cookstove sector
107 that newly incorporates BC as IN is urgently needed.

108 Here, we employ a global aerosol-climate model to quantify the impacts of solid fuel cookstove
109 carbonaceous aerosol emissions globally and from India on global climate change. Sect. 2 presents
110 the Methods including the evaluation measurement data sets for BC, OA and aerosol optical depth
111 (AOD), the model description and experimental design. Sect. 3 details the results of the model
112 evaluation and the impacts of the global and Indian solid fuel cookstove emissions on the
113 atmospheric radiation budget and global climate. Discussion and summary are provided in Sect.
114 4.

115 **2. Methods**

116 **2.1 BC and OC evaluation measurement database**

118 Ground-based BC observations are from IMPROVE (the Interagency Monitoring of PROtected
119 Visual Environment, <http://vista.cira.colostate.edu/Improve/>) for the year 2010 over North
120 America (Malm et al., 1994), EMEP (the European Monitoring and Evaluation Programme,
121 <http://ebas.nilu.no>) for 2009-2013 over Europe, and sporadic measurement campaigns for China
122 and India. Elemental carbon (EC) concentrations are measured using Thermal Optical Reflectance
123 (TOR) (Chow et al., 1993, 2004; EMEP/MSC-W et al., 2014). Our measurement database
124 comprises a total of 152 sites from IMPROVE, 28 sites from EMEP, 35 sites for China, and 41
125 sites for India. The number of urban sites includes 8 from IMPROVE, 5 from EMEP, 17 for China,

126 and 23 for India. Here we define urban (including semi-urban) sites as the geographic locations of
127 the measured sites locating in a city, others as rural sites.

128 A global network of aerosol mass spectrometer (AMS) surface measurements for organic aerosol
129 (OA) for 2000-2008 are used to compare with model simulations (Spracklen et al., 2011a; Zhang
130 et al., 2007; Zheng et al., 2015). The AMS technique measures hydrocarbon-like OA (HOA),
131 oxygenated OA (OOA) and total OA (HOA + OOA). HOA is a surrogate for primary OA (POA)
132 emitted directly from fossil fuel and biomass burning, while OOA is a surrogate for secondary OA
133 (SOA). In this study, we compare monthly mean total OA with model simulated total OA (POA +
134 SOA). The majority of the AMS measurements in the surface concentration database were made
135 prior to 2005.

136 Ground-based AOD observations from AERONET (AErosol RObtic NETwork,
137 <https://aeronet.gsfc.nasa.gov>) during 1993-2016 are applied to examine model skill (Dubovikl and
138 King, 2000; Holben et al., 1998, 2001). A climatological AOD value averaged over 1993-2016 for
139 each site is used to compare with the model simulation. The AERONET version 2 level-2 product
140 is used in this study.

141 **2.2 NCAR CAM5-Chem global model description**

142 We apply the NCAR Community Atmosphere Model version 5.3 with chemistry (CAM5-Chem)
143 within the Community Earth System Model (CESM) version 1.2.2 (Emmons et al., 2010;
144 Lamarque et al., 2012; Tilmes et al., 2015). The oxidant-aerosol system is fully coupled in CAM5-
145 Chem. The horizontal resolution of CAM5-Chem is 0.9° latitude by 1.25° longitude, with 56
146 vertical levels from surface up to about 40 km. In the standard CAM5-Chem, aerosol
147 microphysical processes are represented using a 3-mode scheme (MAM3; aitken, accumulation
148 and coarse modes). MAM3 simulates both mass and number concentrations of aerosols. Aerosol
149 size distributions in each mode are assumed to be lognormal (Liu et al., 2012). The model treats
150 the effects of aerosol acting as CCN in liquid-phase clouds (Ghan et al., 2012). The aerosol
151 components in MAM3 include BC, primary organic matter (POM), secondary organic aerosol
152 (SOA), sulfate, sea salt and dust, which are assumed to be internally mixed within each lognormal
153 mode. Specifically, BC and POM from solid fuel cookstove emissions are treated in the
154 accumulation mode, with size range of 0.058-0.27 μm (Liu et al., 2012). Mass yields of semi-

155 volatile organic gas-phase species (SOAG) from emissions of isoprene, monoterpenes, big alkanes
156 and alkenes, as well as toluene are prescribed (Emmons et al., 2010; Liu et al., 2012; Tilmes et al.,
157 2015). The condensable SOAG reversibly and kinetically partitions into the aerosol phase to form
158 SOA in CAM5-Chem as described in Liu et al. (2012).

159 **2.3 Emissions**

160 Global anthropogenic emissions are from the IIASA (International Institute for Applied System
161 Analysis) Greenhouse Gas-Air Pollution Interactions and Synergies (GAINS) integrated
162 assessment model ECLIPSE V5a (Evaluating the Climate and Air Quality Impacts of Short-lived
163 Pollutants version 5a) for the year 2010 (Amann et al., 2011, 2013; Klimont et al., 2017; Stohl et
164 al., 2015). Species in ECLIPSE V5a include BC, POM, sulfur dioxide, nitrogen oxides, carbon
165 monoxide, volatile organic compounds, and ammonium, with their annual global budgets for the
166 year 2010 shown in Table 1. ECLIPSE V5a emissions available at 0.5° latitude by 0.5° longitude
167 spatial resolutions are re-gridded to the model spatial resolution. ECLIPSE V5a does not include
168 shipping or wildfire biomass burning emissions, which are instead obtained from the IPCC AR5
169 RCP8.5 scenario for the year 2010 (Riahi et al., 2011).

170 **2.4 Simulations: BC not active as IN**

171 Atmosphere-only simulations are performed in specified dynamics (SD) mode with offline
172 meteorological fields from the Goddard Earth Observing System model version 5 (GEOS-5). In
173 this SD mode configuration, the internally derived meteorological fields (e.g., horizontal wind
174 component, air temperature and latent heat flux) are nudged by 10% towards reanalysis fields from
175 GEOS-5 for every model time step. The nudging technique in CAM5-Chem has been evaluated to
176 quantify the aerosol indirect effect in order to reduce the influence of natural variability
177 (Kooperman et al., 2012). Sea surface temperature and sea ice in the model are prescribed from
178 the Climatological/Slab-Ocean Data Model (DOCN) and Climatological Ice Model (DICE)
179 respectively, with monthly-varying decadal mean averaged over 1981-2010.

180 We perform three sets of model simulations using the model configurations shown in Table 2. The
181 first set of simulations represents the control with anthropogenic emissions following ECLIPSE
182 V5a, as described above (hereafter referred to as BASE). The second set of simulations are

183 identical to the BASE simulation except the global solid fuel cookstove emissions for aerosols and
184 gas-phase aerosol and ozone precursors are set to zero (termed as GBLSF_OFF). The third set of
185 simulations is identical to BASE except the solid fuel cookstove emissions are set to zero over the
186 Indian sub-continent (termed as INDSF_OFF). We run all the above simulations for 6 years from
187 2005 to 2010, with the first year discarded as spin-up and the last five years averaged for output
188 analysis. The differences between BASE and GBLSF_OFF isolate the impacts of the global solid
189 fuel cookstove sector aerosol emissions, and the differences between BASE and INDSF_OFF
190 isolate the impacts of the Indian solid fuel cookstove sector aerosol emissions. Top-of-the-
191 atmosphere (TOA) aerosol shortwave (SW) and longwave (LW) radiative effects are calculated
192 using the Rapid Radiative Transfer Model for GCMs (RRTMG) that is coupled to CAM5-Chem
193 (Ghan, 2013; Ghan et al., 2012).

194 **2.5 Simulations: BC active as IN**

195 In default CAM5-Chem, BC is not treated as IN (Liu et al., 2012; Tilmes et al., 2015). IN
196 concentrations from homogeneous nucleation are calculated as a function of vertical velocity (Liu
197 et al., 2007). Several lab and field studies indicate that BC particles can act as IN (Cozic et al.,
198 2008; DeMott et al., 1999; Koehler et al., 2009; Kulkarni et al., 2016). Therefore, we conduct
199 additional simulations that treat BC as an effective IN applying the ice nucleation scheme of
200 Barahona and Nenes (2008, 2009). The scheme estimates maximum supersaturation and ice crystal
201 concentrations and considers competition between homogeneous and heterogeneous freezing.
202 Homogeneous nucleation occurs in solution droplets formed on soluble aerosols (mainly sulfate),
203 while heterogeneous nucleation occurs on IN, which here are a small subset of mineral dust and
204 black carbon particles. The heterogeneous freezing of BC and dust is described as a generalized
205 ice nucleation spectrum.

206 We perform three additional model simulations, with model configurations identical to those in
207 Table 2, except for the treatment of BC particles as effective IN. In addition, for each model
208 simulation, we alter the plausible maximum freezing efficiency (MFE) of BC as 0.01, 0.05 and 0.1
209 that provides an uncertainty range in the global climatic impact assessment.

210 **3 Results**

211 **3.1 Evaluation of surface BC and OA concentrations**

212 Surface observation networks from IMPROVE, EMEP, and various campaigns in China and India
 213 are employed to compare with model simulations, as shown in Figure 1. We diagnose the
 214 normalized mean bias (NMB) for each source region, calculated as

$$215 \quad \text{NMB} = \left(\frac{\sum_i (M_i - O_i)}{\sum_i O_i} \right) \times 100\% \quad (1)$$

216 where M and O represent monthly mean model simulated and observational concentrations at site
 217 i respectively, and \sum is the sum over all the sites within a source region.

218 In general, the model simulated surface BC concentrations agree with observations to within a
 219 factor of 2, consistent with previous studies (Huang et al., 2013; Wang et al., 2011, 2014a, 2014b).
 220 A total of 41 surface BC observational sites are used to evaluate the model simulation over India
 221 (Fig. 1a). On average, the model underestimates surface BC concentrations by approximately 45%
 222 and 34% over urban and rural sites respectively, with a total NMB -41% (Fig. 1a), which implies
 223 a marked underestimation of the BC emissions in India. Previous modeling studies have also
 224 reported large underestimates of BC surface concentrations over India against observations
 225 (Gadhavi et al., 2015; He et al., 2014; Zhang et al., 2015). Part of the model/measurement
 226 discrepancy is related to a sampling bias because the majority of the observations are located over
 227 urban or heavily polluted regions. For China sites, the NMB value is -16% (Fig. 1b). Similar to
 228 India, the model substantially underestimates the surface BC concentrations over urban sites with
 229 a NMB of -30%. However, the model performs relatively well over rural areas, with a NMB close
 230 to zero. For IMPROVE, the NMB values for rural and urban sites are -15% and -43%, respectively,
 231 with a total NMB -28% (Fig. 1c). Over Europe, the model simulated surface BC concentrations
 232 agree quite well with observations, with a NMB value of -8%, although two urban sites show
 233 substantial model underestimation (Fig. 1d).

234 The 40 AMS surface OA measurements are grouped into three categories: East Asia (8 sites),
 235 North America (17 sites) and Europe (15 sites) (Spracklen et al., 2011a; Zhang et al., 2007; Zheng
 236 et al., 2015). Figure 2 shows the evaluation of simulated surface OA against observations. Over
 237 East Asia, the model slightly underestimates observed OA, with a NMB of $-8.5 \pm 5\%$ (\pm represents
 238 modeled temporal standard deviations for n=5 run years) (Fig. 2a). In contrast, the simulated OA
 239 concentrations overestimate the measurements by over a factor of 2 in North America, with a NMB

value of $124 \pm 24\%$ (Fig. 2b). For the European sites, we find a simulated OA overestimation of measured concentrations by up to $0.9 \pm 0.7 \mu\text{g m}^{-3}$, corresponding to a NMB of $+32 \pm 26\%$ (Fig. 2c).

3.2 Evaluation of model AOD

Figure 3 compares simulated AOD values against observations over nine regions across the globe, including India, China, Rest of Asia (excluding China and India), Africa, South America, North America, Europe, Australia and remote regions. Over India, the simulated annual mean AOD is lower than observations by about $16 \pm 3\%$ (Fig. 3a), with large bias sources mainly from the northern India regions (e.g., New Delhi and Kanpur). This is consistent with Quennehen et al. (2016) who also reported that model simulated AOD values were generally lower than satellite-derived AOD over northern India, using the same emission inventory as our study. As discussed in Sect. 3.1, model simulated surface BC concentrations over India are also underestimated (by up to 41%), therefore, the low bias of model simulated AOD can be attributed, in part, to the underestimation of Indian BC emissions from ECLIPSE V5a emission inventory (Stohl et al., 2015), although global anthropogenic BC budgets in ECLIPSE V5a lie in the high end compared with previous studies (Bond et al., 2004, 2013; Janssens-Maenhout et al., 2015). The model underestimate of AOD from AERONET in India may also be related to the fairly coarse global model resolution, as previously reported by Pan et al. (2015) and Zhang et al. (2015). A similar pattern is found over China (Fig. 3b) and the rest of Asia (Fig. 3c), with NMB values of $-21 \pm 4\%$ and $-15 \pm 6\%$ respectively. Model simulated AOD values from several sites in West Asia (Fig. 3c) are higher than observations, which is probably caused by the model overestimation of dust emissions (He and Zhang, 2014). This directly leads to annual mean model simulated AOD values over Africa $25 \pm 11\%$ higher than observations because Saharan dust emissions dominate the AOD over North Africa (Fig. 3d). For South America, the model generally agrees quite well with observations (Fig. 3e), except for a few sites where model simulated AOD values are lower than observations by more than a factor of 2. This is probably due to the model underestimation of biomass burning emissions there (Reddington et al., 2016). AOD values over North America (Fig. 3f) and Europe (Fig. 3g) are relatively lower (with values generally < 0.3), due to lower anthropogenic emissions. In these two regions, modeled AOD agrees with observations within a factor of 2, with NMB values $-20 \pm 4\%$ and $-18 \pm 9\%$ respectively. CAM5-Chem overestimates

270 AOD over Australia (Fig. 3h) and remote sites (Fig. 3i), with NMB values of $+69 \pm 17\%$ and $+47$
271 $\pm 12\%$, respectively. Globally, model simulated AOD agrees quite well with observations, with
272 NMB values close to zero.

273 3.3 Contribution of solid fuel cookstove sector emissions to atmospheric BC and POM

274 3.3.1 BC

275 Annual BC emissions and budgets are reported in Table 3 based on the anthropogenic inventory
276 from ECLIPSE V5a. Annual BC emissions from the global and Indian solid fuel cookstove
277 emissions are 2.31 and 0.36 Tg yr^{-1} , accounting for 23.7% and 3.7% of the total BC emissions. For
278 the control simulation, global annual mean BC burden and lifetime are $0.12 \pm 0.001 \text{ Tg}$ and $4.5 \pm$
279 0.04 days, respectively (Table 3), at the low end of the range estimated by AeroCom (Schulz et
280 al., 2006; Textor et al., 2006).

281 Figure 4 shows the zonal mean BC concentrations from the control simulation (Fig. 4a), global
282 (Fig. 4b) and Indian (Fig. 4c) solid fuel cookstove emissions respectively. For the control
283 simulation, in general, the highest BC concentrations (by up to $0.40 \mu\text{g m}^{-3}$) occur at the surface
284 over the emission source regions in the mid-latitudes (e.g., China and India). In the tropics and
285 mid-latitudes, zonal mean BC concentrations decrease with increasing altitude, due to wet removal
286 and deposition, as found in Huang et al. (2013). A similar vertical distribution is observed for the
287 impacts from global and Indian solid fuel cookstove emissions, although the magnitude is smaller,
288 compared with the control simulation. Annual mean BC burdens from global and Indian solid fuel
289 cookstove emissions account for about $24.2 \pm 0.7\%$ and $5.0 \pm 0.0\%$ of that in the control simulation
290 ($0.12 \pm 0.001 \text{ Tg}$).

291 3.3.2 POM

292 Global POM emissions are mainly from biomass burning (31 Tg yr^{-1}) and anthropogenic emissions
293 (18.9 Tg yr^{-1}), with global and Indian solid fuel cookstove emissions accounting for, 21% and
294 3.4% respectively, of the total POM emissions (Table 3). In our control simulation, the annual
295 mean POM burden is $0.66 \pm 0.006 \text{ Tg}$, and the global annual mean POM lifetime is 4.8 ± 0.04
296 days (Table 3).

297 In Figure 5, we show the annual zonal mean POM concentrations for the control simulation (Fig.
 298 5a) and for global (Fig. 5b) and Indian (Fig. 5c) solid fuel cookstove emissions. There are two
 299 maxima in the annual zonal mean POM concentrations near the surface. One is located in the
 300 tropics due to the large biomass burning emissions there, and the other is located over mid-latitude
 301 regions and originates mainly from anthropogenic emissions (Chung and Seinfeld, 2002; Huang
 302 et al., 2013). For POM concentrations from global solid fuel cookstove emissions, a single
 303 maximum is evident in the Northern Hemisphere (NH) subtropics at the surface (Fig. 5b). The
 304 surface maximum for the Indian solid fuel cookstove emissions reaches a maximum in the NH
 305 subtropics. The annual mean POM burdens from global and Indian solid fuel cookstove emissions
 306 are 0.13 ± 0.004 Tg and 0.027 ± 0.002 Tg respectively.

307 3.4 Impacts of solid fuel cookstove aerosol emissions on global radiation budget

Deleted: climate change

308 3.4.1 Direct radiative effect (DRE)

310 The DRE impacts of the global and Indian solid fuel cookstove emissions are shown in Figure 6.
 311 For the global solid fuel cookstove sector, the globally averaged DRE from aerosol emissions is
 312 $+70 \pm 3$ mW m⁻² (\pm represents modeled temporal standard deviations for n=5 run years) without
 313 treating BC as IN, which is a warming effect. The positive DRE from global solid fuel cookstove
 314 emissions shows large spatial variability, with the largest impacts located over western Africa,
 315 followed by India and China (figure not shown). The contributions of BC and POM to DRE are
 316 $+105 \pm 4$ (warming) and -14 ± 1 (cooling) mW m⁻², respectively. In other words, the warming
 317 effect of BC is partially offset by the cooling effect from POM. Additional cooling effects may
 318 come from sulfate and SOA. CAM5-Chem assumes that BC is internally mixed with other
 319 components in the accumulation mode and simulates enhanced absorption (BC mass absorption
 320 cross section = 14.6 m² g⁻¹) when BC is coated by soluble aerosol components and water vapor
 321 (Ghan et al., 2012), which results in larger estimates of the DRE than for BC alone (Bond et al.,
 322 2013; Jacobson, 2001b).

323 The DRE from Indian solid fuel cookstove emissions also corresponds to a net warming effect
 324 (Fig. 6), with a global annual mean value of $+11 \pm 1$ mW m⁻². Large impacts are found over
 325 continental India, the Tibetan Plateau and southeastern China. On a global annual basis, DRE

327 values from BC and POM emissions from the Indian solid fuel cookstove sector are $+18 \pm 1$ and -
328 $3 \pm 0.2 \text{ mW m}^{-2}$, respectively.

329 3.4.2 Aerosol indirect, semi-direct and surface albedo effects: BC not active as IN

330 Global annual mean AIE and SAE values from global and Indian solid fuel cookstove aerosol
331 emissions are shown in Figure 6. In our study, AIE includes the first (albedo) and second (lifetime)
332 indirect effects, as well as the semi-direct effect. Annually averaged AIE from the global solid fuel
333 cookstove sector is $-226 \pm 5 \text{ mW m}^{-2}$ (Fig. 6), with annual mean shortwave (SW) AIE -122 ± 22
334 mW m^{-2} and longwave (LW) AIE $-104 \pm 17 \text{ mW m}^{-2}$, without treating BC as IN. Both the annual
335 mean SW and LW AIE thus yield cooling effects. The cooling signals of SW AIE mainly occur
336 over the western coast of South America, west and east coasts of Africa, South China and Himalaya
337 regions (figure not shown). This is directly linked to the contribution of global solid fuel cookstove
338 aerosol emissions to CCN (Pierce et al., 2007), which increases the cloud droplet number
339 concentrations (CDNC) and cloud liquid water path (CLWP). Figure 7 shows the global vertically-
340 integrated distribution of CLWP from the contribution of global solid fuel cookstove aerosol
341 emissions. The higher CLWP is due to the enhanced lifetime of liquid and mixed-phase clouds,
342 which therefore reflect more solar radiation, leading to cooling effect. For the LW AIE, the largest
343 cooling effect is found over tropical regions, especially over southern India and the Indian Ocean.
344 In order to investigate the causes of the LW AIE cooling effect, we analyze the cloud fraction
345 change over a defined region (Latitude:0-20°N; Longitude:60-90°E) due to the effect from the
346 global solid fuel cookstove sector. As shown in Figure 8a, cloud fraction in the lower troposphere
347 increases. However, in the middle and upper troposphere cloud fraction decreases by up to 0.6%,
348 with the strongest decrease found at ~150 hPa. We further analyze the changes in shallow and deep
349 convective mass fluxes of moisture over the same domain. As shown in Figure 8b, moist shallow
350 convective mass flux generally shows increases in the lower troposphere, which means that solid
351 fuel cookstove aerosol emissions enhance the convective transport of water vapor within the
352 boundary layer. By contrast, the deep convective mass flux demonstrates decreases from surface
353 up to the middle troposphere (Fig. 8c). This indicates that solid fuel cookstove aerosol emissions
354 may stabilize the boundary layer and inhibit the transport of water vapor from the surface to the
355 upper troposphere/lower stratosphere, which leads to decreases in ice cloud formation, thus

356 reducing cloud cover in the upper troposphere and lower stratosphere (UTLS) region at around
357 200 hPa (Fig. 8a) and a LW AIE cooling effect.

358 The global annual mean AIE from Indian solid fuel cookstove aerosol emissions accounts for
359 approximately 10% ($-22 \pm 3 \text{ mW m}^{-2}$) relative to the value of AIE from the global solid fuel
360 cookstove sector (Fig. 6), with globally averaged SW and LW AIE values of -3 ± 11 and -19 ± 11
361 mW m^{-2} respectively.

362 Global annual mean SAE values from global and Indian solid fuel cookstove sector are relatively
363 small: $+15 \pm 3$ and $-2 \pm 3 \text{ mW m}^{-2}$, respectively (Fig. 6). The warming effect is mainly due to the
364 deposition of BC on the surface of snow and sea ice (Flanner et al., 2007; Ghan, 2013; Ghan et al.,
365 2012).

366 3.4.3 Total radiative effect: BC not active as IN

367 The net total radiative effect of global and Indian solid fuel cookstove aerosol emissions are both
368 cooling, with the global annual mean estimated to be -141 ± 4 and $-12 \pm 4 \text{ mW m}^{-2}$ respectively
369 (Fig. 6). This suggests that if we remove solid fuel cookstove aerosol emissions, it will result in
370 warming and thus slightly increased global surface air temperature. That being said, this is likely
371 to be quite sensitive to model representation of aerosol mixing state (Fierce et al., 2017).

372 3.4.4 Total radiative effect: BC active as IN

373 For the radiative effect of global solid fuel cookstove emissions with BC as IN, global annual mean
374 DRE is $105 \pm 13 \text{ mW m}^{-2}$ (\pm represents standard deviations from modeling results with BC MFE
375 values as 0.01, 0.05 and 0.1), ranging from +90 to +115 mW m^{-2} , which is 29-64% higher than the
376 DRE values from the default scheme (Fig. 6). Intriguingly, large globally averaged negative SW
377 AIE ($-1.36 \pm 0.63 \text{ W m}^{-2}$) and positive LW AIE ($+1.18 \pm 0.44 \text{ W m}^{-2}$) for global solid fuel
378 cookstove aerosol emissions are found, with annual mean values for the SW AIE ranging from -
379 1.83 to -0.64 W m^{-2} and from +0.67 to +1.45 W m^{-2} for the LW AIE. This results in a rather
380 uncertain net AIE, with a global annual mean AIE of $-177 \pm 223 \text{ mW m}^{-2}$ (Fig. 6). The reason for
381 the large global annual average negative SW AIE and positive LW AIE is a substantial increase in
382 high cloud ($< 500 \text{ hPa}$) fractions when BC acts as an efficient IN. For instance, with MFE = 0.1,
383 large increases (by up to 9%) in high cloud fractions from global solid fuel cookstove aerosol

emissions are found over subtropical regions, especially over the southern Atlantic Ocean (Fig. 9). With BC particles active as IN, ice particle sizes become smaller, leading to a slower settling velocity for ice particles and thus an increase in the lifetime of ice clouds. Increases in high clouds not only reflect more solar radiation back to space, but also trap more LW radiation within the troposphere. For SAE, the global annual mean value is $+12 \pm 10 \text{ mW m}^{-2}$ (Fig. 6). As a result, the net total radiative effect of global solid fuel cookstove aerosol emissions ranges from -275 to +154 mW m^{-2} , with a global annual mean of $-59 \pm 215 \text{ mW m}^{-2}$ (Fig. 6). Again, the source of the large uncertainty of the total radiative effect is due to the choice of MFE values. With $\text{MFE} = 0.01$, the global mean LW AIE ($+672 \text{ mW m}^{-2}$) outweighs SW AIE (-638 mW m^{-2}), and therefore results in a net warming effect. For other MFE values (0.05 and 0.1), the absolute global annual mean SW AIE values are always higher than the LW AIE, leading to a net negative (i.e., cooling) total radiative effect.

For the Indian solid fuel cookstove sector, the global annual mean net total radiative effect is $0.3 \pm 29 \text{ mW m}^{-2}$, with an AIE of -18 ± 37 and a SAE of $+1 \pm 8 \text{ mW m}^{-2}$, respectively.

4 Discussion and Summary

In this study, we employ the atmospheric component of a global 3-D climate model CESM v1.2.2, CAM5.3-Chem, to investigate the impacts of solid fuel cookstove emissions on global climate change. We update the default anthropogenic emission inventory using IIASA ECLIPSE V5a for the year 2010. We focus our analysis on the radiative effects of global and Indian solid fuel cookstove aerosol emissions. Model performance is evaluated against a global dataset of BC and OA measurements from surface sites and AOD from AERONET. Compared with observations, the model successfully reproduces the spatial patterns of atmospheric BC and OA concentrations, and generally agrees with measurements to within a factor of 2. Globally, the simulated AOD agrees quite well with observations, with NMB values close to zero. Nevertheless, the model tends to underestimate AOD values over source regions (except for Africa) and overestimate AOD over remote regions. The underestimates of AOD over India and China indicate that anthropogenic emissions of carbonaceous aerosols and sulfate precursors in ECLIPSE V5a are underestimated because carbonaceous aerosols and sulfate account for over 60% of the AOD over these two countries (Lu et al., 2011; Streets et al., 2009), which may introduce uncertainties for our climate

estimates. The simulations reflect a present-day climatology forced with recycled year 2010 anthropogenic emissions. Model simulated BC concentrations were sampled in exact correspondence to the observed temporal period. In some limited cases, OA and AOD are not exactly temporally consistent with the available aerosol measurement network climatologies applied in the evaluation. For regions where carbonaceous aerosol emissions have undergone substantial changes over short periods in the past few years, the model-measurement comparison may therefore introduce additional uncertainty. However, we focus the evaluation on the large-scale regional aerosol system dynamics. In the control simulation, the global annual mean BC burden and lifetime are 0.12 ± 0.001 Tg and 4.5 ± 0.04 days. For POM, the burden and lifetime are 0.66 ± 0.006 Tg and 4.8 ± 0.04 days. Annual mean surface BC (POM) concentrations over Northern India, East China and sub-Saharan Africa are 1.55 ± 0.076 , 0.76 ± 0.028 and 0.11 ± 0.004 $\mu\text{g m}^{-3}$ (7.11 ± 0.32 , 3.95 ± 0.12 and 0.48 ± 0.02 $\mu\text{g m}^{-3}$), respectively. BC and POM burdens from global solid fuel cookstove emissions are 0.029 ± 0.001 and 0.13 ± 0.004 Tg, while contributions from the Indian sector are 0.006 ± 0.000 and 0.027 ± 0.004 Tg, respectively.

In the default CESM simulations without treating BC as IN, globally averaged DRE values from global and Indian solid fuel cookstove emissions are $+70 \pm 3$ and $+11 \pm 1$ mW m^{-2} , respectively. The contributions of BC and POM from global solid fuel cookstove emissions to the DRE are $+105 \pm 4$ and -14 ± 1 mW m^{-2} . Global annual mean SW and LW AIE values from global solid fuel cookstove emissions are -122 ± 22 and -104 ± 17 mW m^{-2} , with contributions from India yielding -3 ± 11 mW m^{-2} for the SW AIE and -19 ± 11 mW m^{-2} for the LW AIE, respectively. The cooling effect of the SW AIE is associated with the increases of CCN and CDNC, whereas the negative effects of LW AIE are caused by the suppression of convection that transports water vapor from lower troposphere to upper troposphere/stratosphere, thus reducing ice cloud cover. The CAM5-Chem also computes the SAE, with global and Indian solid fuel cookstove emissions contributing $+15 \pm 3$ and -2 ± 3 mW m^{-2} , respectively. As a result, the net total radiative effects of global and Indian solid fuel cookstove emissions are -141 ± 4 and -12 ± 4 mW m^{-2} , respectively, both producing a net cooling effect.

Sensitivity studies are carried out to examine the impacts of global and Indian solid fuel cookstove emissions on climate by treating BC as an effective IN, with MFE as 0.01, 0.05 and 0.1, respectively. For the radiative impacts of global solid fuel cookstove emissions, global annual

Deleted: climate

mean DRE is $+105 \pm 13 \text{ mW m}^{-2}$, which is $\sim 50\%$ higher than the default model scheme in which BC particles are not treated as IN (Fig. 6). This is driven by the increases of BC burden (due to prolonged BC lifetimes) from global solid fuel cookstove emissions by up to 17% with BC as IN. Because the BC absorption effect dominates the DRE, increases in BC burden enhance the magnitude of annual mean DRE (Jacobson, 2001a). Compared with the default model scheme, significant changes in globally averaged SW AIE are found, with a global annual mean of $-1.36 \pm 0.63 \text{ W m}^{-2}$, which is about an order of magnitude higher than that from the default scheme. Moreover, in contrast to the cooling effect found in the default scheme, annual mean positive LW AIE is simulated here ($+1.18 \pm 0.44 \text{ W m}^{-2}$). The above changes in cookstove emission induced SW and LW AIE are caused by the substantial increases in high cloud ($< 500 \text{ hPa}$) fractions with BC particles acting as IN by up to 9% due to the effect of solid fuel cookstove emissions. Large increases in high cloud fractions are found mainly over tropical regions, especially over southern Africa. For the SAE, similar to the model default scheme, the global annual mean value is $+12 \pm 10 \text{ mW m}^{-2}$. Summing up the DRE, the AIE and the SAE, the net total radiative effect of global solid fuel cookstove emissions is $-59 \pm 215 \text{ mW m}^{-2}$. For the Indian sector, the global mean total radiative effect is $0.3 \pm 29 \text{ mW m}^{-2}$, with a net AIE -18 ± 37 and a SAE $+1 \pm 8 \text{ mW m}^{-2}$, respectively.

We compare our simulation results with previous studies as shown in Figure 10. The globally averaged DRE in our control simulation is more than four times higher than that from the baseline simulation of Kodros et al. (2015), which assumes homogeneous particle mixing state (Fig. 10). Annual emissions of BC from global solid fuel cookstove sector in our study (2.3 Tg C yr^{-1}) is approximately 44% higher than that from global biofuel emissions (1.6 Tg C yr^{-1}) in Kodros et al. (2015), which, to some extent, leads to differences in annual mean DRE values together with different optical calculations. The annual mean DRE value from another study by Butt et al. (2016) differs from ours in magnitude and sign, and concluded that annually averaged DRE from residential combustion sources was -5 mW m^{-2} (Fig. 10). The negative effect of DRE in Butt et al. (2016) is partially driven by the inclusion of SO_2 emissions ($8.9 \text{ Tg SO}_2 \text{ yr}^{-1}$) from commercial coal combustion in the residential sector, leading to the cooling effect of sulfate and organic aerosols outweighing the warming from BC. For AIE, our control simulation is 38 times higher than that from Kodros et al. (2015) and over an order of magnitude higher than that from Butt et al. (2016). Consistent with our study, Ward et al. (2012) also found a large AIE (-1.74 to 1.00 W

475 m⁻²) for carbonaceous aerosols from fires using CESM CAM4-Chem. Both Kodros et al. (2015)
476 and Butt et al. (2016) used offline radiative models to calculate AIE and only considered the first
477 (albedo) aerosol indirect effect, which may partially explain the AIE differences. As mentioned
478 earlier, the AIE in our study includes aerosol first and second indirect effects as well as the semi-
479 direct effect. Lacey and Henze (2015) estimated that the global surface air temperature changes
480 due to solid wood fuel removal ranged from -0.28 K (cooling) to +0.16 K (warming), with a central
481 estimate of -0.06 K (cooling). This cooling estimate is opposite to our study. However, we
482 acknowledge that there are fundamental differences in calculating the radiative effect between our
483 study and Lacey and Henze (2015), which employed absolute regional temperature potentials to
484 quantify the climate responses.

485 Cookstove intervention programs have been implemented in developing countries, such as China,
486 India and some African countries, to improve air quality and human health and to mitigate climate
487 change (Anenberg et al., 2017; Aung et al., 2016; Carter et al., 2016). Our results suggest that
488 large-scale efforts to replace inefficient cookstoves in developing countries with advanced
489 technologies is not likely to reduce global warming through aerosol reductions, and may even lead
490 to increased global warming when aerosol-cloud interactions are taken into account. Therefore,
491 without improved constraints on BC interactions with clouds, especially mixed-phase and ice
492 clouds, the net sign of the impacts of carbonaceous aerosols from solid fuel cookstoves on global
493 climate (warming or cooling) remains ambiguous. This study does not include the greenhouse gas
494 emission effects from the solid fuel cookstove sector, which may indeed be large enough to imply
495 a net warming global climate impact depending on time scale (Lacey et al., 2017).

496 **Acknowledgements**

497 This article was developed under Assistance Agreement No. R835421 awarded by the U.S.
498 Environmental Protection Agency to SEI. It has not been formally reviewed by EPA. The views
499 expressed in this document are solely those of the authors and do not necessarily reflect those of
500 the Agency. EPA does not endorse any products or commercial services mentioned in this
501 publication. N. Unger acknowledges support from the University of Exeter, UK. The authors are
502 grateful to R. Bailis, A. Grieshop, J. Marshall, and H. Zerrieffi for helpful discussions and
503 conversations that guided the manuscript development. We are thankful for helpful discussions

504 with S. Tilmes and S. Ghan. This project was supported in part by the facilities and staff of the
505 Yale University High Performance Computing Center.

506 **References**

- 507 Amann, M., Bertok, I., Borken-Kleefeld, J., Cofala, J., Heyes, C., Höglund-Isaksson, L.,
508 Klimont, Z., Nguyen, B., Posch, M., Rafaj, P., Sandler, R., Schöpp, W., Wagner, F. and
509 Winiwarter, W.: Cost-effective control of air quality and greenhouse gases in Europe: Modeling
510 and policy applications, *Environ. Model. Softw.*, 26(12), 1489–1501,
511 doi:10.1016/j.envsoft.2011.07.012, 2011.
- 512 Amann, M., Klimont, Z. and Wagner, F.: Regional and Global Emissions of Air Pollutants:
513 Recent Trends and Future Scenarios, *Annu. Rev. Environ. Resour.*, 38(1), 31–55,
514 doi:10.1146/annurev-environ-052912-173303, 2013.
- 515 Anenberg, S. C., Henze, D. K., Lacey, F., Irfan, A., Kinney, P., Kleiman, G. and Pillarisetti, A.:
516 Air pollution-related health and climate benefits of clean cookstove programs in Mozambique,
517 *Environ. Res. Lett.*, 12(2), 25006, doi:10.1088/1748-9326/aa5557, 2017.
- 518 Archer-Nicholls, S., Carter, E., Kumar, R., Xiao, Q., Liu, Y., Frostad, J., Forouzanfar, M. H.,
519 Cohen, A., Brauer, M., Baumgartner, J. and Wiedinmyer, C.: The regional impacts of cooking
520 and heating emissions on ambient air quality and disease burden in China, *Environ. Sci.*
521 *Technol.*, 50(17), 9416–9423, doi:10.1021/acs.est.6b02533, 2016.
- 522 Aung, T. W., Jain, G., Sethuraman, K., Baumgartner, J., Reynolds, C., Grieshop, A. P., Marshall,
523 J. D. and Brauer, M.: Health and Climate-Relevant Pollutant Concentrations from a Carbon-
524 Finance Approved Cookstove Intervention in Rural India, *Environ. Sci. Technol.*, 50(13), 7228–
525 7238, doi:10.1021/acs.est.5b06208, 2016.
- 526 Barahona, D. and Nenes, A.: Parameterization of cirrus cloud formation in large-scale models:
527 Homogeneous nucleation, *J. Geophys. Res. Atmos.*, 113(11), 1–15, doi:10.1029/2007JD009355,
528 2008.
- 529 Barahona, D. and Nenes, A.: Parameterizing the competition between homogeneous and
530 heterogeneous freezing in ice cloud formation – polydisperse ice nuclei, *Atmos. Chem. Phys.*, 9,

531 5933–5948, doi:10.5194/acp-9-5933-2009, 2009.

532 Bauer, S. E., Menon, S., Koch, D., Bond, T. C. and Tsigaridis, K.: A global modeling study on
533 carbonaceous aerosol microphysical characteristics and radiative effects, *Atmos. Chem. Phys.*,
534 10(15), 7439–7456, doi:10.5194/acp-10-7439-2010, 2010.

535 Bond, T., Venkataraman, C. and Masera, O.: Global atmospheric impacts of residential fuels,
536 *Energy Sustain. Dev.*, 8(3), 20–32, doi:10.1016/S0973-0826(08)60464-0, 2004.

537 Bond, T. C., Doherty, S. J., Fahey, D. W., Forster, P. M., Bernsten, T., Deangelo, B. J., Flanner,
538 M. G., Ghan, S., Kärcher, B., Koch, D., Kinne, S., Kondo, Y., Quinn, P. K., Sarofim, M. C.,
539 Schultz, M. G., Schulz, M., Venkataraman, C., Zhang, H., Zhang, S., Bellouin, N., Guttikunda,
540 S. K., Hopke, P. K., Jacobson, M. Z., Kaiser, J. W., Klimont, Z., Lohmann, U., Schwarz, J. P.,
541 Shindell, D., Storelvmo, T., Warren, S. G. and Zender, C. S.: Bounding the role of black carbon
542 in the climate system: A scientific assessment, *J. Geophys. Res. Atmos.*, 118(11), 5380–5552,
543 doi:10.1002/jgrd.50171, 2013.

544 Bonjour, S., Wolf, J. and Lahiff, M.: Solid Fuel Use for Household Cooking: Country and
545 Regional Estimates for 1980–2010, *Environ. Health Perspect.*, 121(7), 784–790,
546 doi:10.1289/ehp.1205987, 2013.

547 Boucher, O., Randall, D., Artaxo, P., Bretherton, C., Feingold, G., Forster, P., Kerminen, V.-M.
548 V.-M., Kondo, Y., Liao, H., Lohmann, U., Rasch, P., Satheesh, S. K., Sherwood, S., Stevens, B.,
549 Zhang, X. Y. and Zhan, X. Y.: Clouds and Aerosols, *Clim. Chang. 2013 Phys. Sci. Basis.*
550 *Contrib. Work. Gr. I to Fifth Assess. Rep. Intergov. Panel Clim. Chang.*, 571–657,
551 doi:10.1017/CBO9781107415324.016, 2013.

552 Butt, E. W., Rap, A., Schmidt, A., Scott, C. E., Pringle, K. J., Reddington, C. L., Richards, N. A.
553 D., Woodhouse, M. T., Ramirez-Villegas, J., Yang, H., Vakkari, V., Stone, E. A., Rupakheti, M.,
554 Praveen, P. S., Van Zyl, P. G., Beukes, J. P., Josipovic, M., Mitchell, E. J. S., Sallu, S. M.,
555 Forster, P. M. and Spracklen, D. V.: The impact of residential combustion emissions on
556 atmospheric aerosol, human health, and climate, *Atmos. Chem. Phys.*, 16(2), 873–905,
557 doi:10.5194/acp-16-873-2016, 2016.

558 Carter, E., Archer-Nicholls, S., Ni, K., Lai, A. M., Niu, H., Secrest, M. H., Sauer, S. M., Schauer,
 559 J. J., Ezzati, M., Wiedinmyer, C., Yang, X. and Baumgartner, J.: Seasonal and Diurnal Air
 560 Pollution from Residential Cooking and Space Heating in the Eastern Tibetan Plateau, *Environ.*
 561 *Sci. Technol.*, 50(15), 8353–8361, doi:10.1021/acs.est.6b00082, 2016.

562 Chow, J. C., Watson, J. G., Pritchett, L. C., Pierson, W. R., Frazer, C. A. and Purcell, R. G.: THE
 563 DRI THERMAL/OPTICAL REFLECTANCE CARBON ANALYSIS SYSTEM :
 564 DESCRIPTION, EVALUATION A N D APPLICATIONS IN U.S. AIR QUALITY STUDIES,
 565 *Atmos. Environ.*, 27A(8), 1185–1201, 1993.

566 Chow, J. C., Watson, J. G., Chen, L.-W. A., Arnott, W. P. and Moosmuller, H.: Equivalence of
 567 Elemental Carbon by Thermal/Optical Reflectance and Transmittance with Different
 568 Temperature Protocols, *Environ. Sci. Technol.*, 38(16), 4414–4422, 2004.

569 Chung, S. H.: Climate response of direct radiative forcing of anthropogenic black carbon, *J.*
 570 *Geophys. Res.*, 110(D11), D11102, doi:10.1029/2004JD005441, 2005.

571 Chung, S. H. and Seinfeld, J. H.: Global distribution and climate forcing of carbonaceous
 572 aerosols, *J. Geophys. Res. Atmos.*, 107(19), doi:10.1029/2001JD001397, 2002.

573 Chylek, P. and Wong, J.: Effect of absorbing aerosols on global radiation budget, *Geophys. Res.*
 574 *Lett.*, 22(8), 929–931, 1995.

575 Cozic, J., Mertes, S., Verheggen, B., Cziczo, D. J., Gallavardin, S. J., Walter, S., Baltensperger,
 576 U. and Weingartner, E.: Black carbon enrichment in atmospheric ice particle residuals observed
 577 in lower tropospheric mixed phase clouds, *J. Geophys. Res. Atmos.*, 113(15), 1–11,
 578 doi:10.1029/2007JD009266, 2008.

579 DeMott, P. J., Chen, Y., Kreidenweis, S. M., Rogers, D. C. and Sherman, D. E.: Ice formation by
 580 black carbon particles, *Geophys. Res. Lett.*, 26(16), 2429–2432, doi:10.1029/1999GL900580,
 581 1999.

582 Dubovikl, O. and King, M. D.: A flexible inversion algorithm for retrieval of aerosol optical
 583 properties from Sun and sky radiance measurements, *J. Geophys. Res.*, 105696(27), 673–20,
 584 doi:10.1029/2000JD900282, 2000.

585 EMEP/MSC-W, EMEP/CCC, EMEP/CEIP, IDAEA-CSIC, CCE/RIVM and FMI:
586 Transboundary particulate matter, photo-oxidants, acidifying and eutrophying components.,
587 2014.

588 Emmons, L. K., Walters, S., Hess, P. G., Lamarque, J.-F., Pfister, G. G., Fillmore, D., Granier,
589 C., Guenther, A., Kinnison, D., Laepple, T., Orlando, J., Tie, X., Tyndall, G., Wiedinmyer, C.,
590 Baughcum, S. L. and Kloster, S.: Description and evaluation of the Model for Ozone and Related
591 chemical Tracers, version 4 (MOZART-4), *Geosci. Model Dev.*, 3, 43–67, doi:10.5194/gmd-3-
592 43-2010, 2010.

593 Ezzati, M. and Kammen, D. M.: The health impacts of exposure to indoor air pollution from
594 solid fuels in developing countries: Knowledge, gaps, and data needs, *Environ. Health Perspect.*,
595 110(11), 1057–1068, doi:10.1289/ehp.021101057, 2002.

596 Fierce, L., Riemer, N. and Bond, T. C.: Toward reduced representation of mixing state for
597 simulating aerosol effects on climate, *Bull. Am. Meteorol. Soc.*, 98(5), 971–980,
598 doi:10.1175/BAMS-D-16-0028.1, 2017.

599 Flanner, M. G., Zender, C. S., Randerson, J. T. and Rasch, P. J.: Present-day climate forcing and
600 response from black carbon in snow, *J. Geophys. Res. Atmos.*, 112(11), 1–17,
601 doi:10.1029/2006JD008003, 2007.

602 Gadhavi, H. S., Renuka, K., Ravi Kiran, V., Jayaraman, A., Stohl, A., Klimont, Z. and Beig, G.:
603 Evaluation of black carbon emission inventories using a Lagrangian dispersion model - A case
604 study over southern India, *Atmos. Chem. Phys.*, 15(3), 1447–1461, doi:10.5194/acp-15-1447-
605 2015, 2015.

606 Garland, C., Delapena, S., Prasad, R., L'Orange, C., Alexander, D. and Johnson, M.: Black
607 carbon cookstove emissions: A field assessment of 19 stove/fuel combinations, *Atmos. Environ.*,
608 169, 140–149, doi:10.1016/j.atmosenv.2017.08.040, 2017.

609 GBD 2015 Risk Factors Collaborators: Global, regional, and national comparative risk
610 assessment of 79 behavioural, environmental and occupational, and metabolic risks or clusters of
611 risks, 1990–2015: a systematic analysis for the Global Burden of Disease Study 2015, *Lancet*,

612 388(10053), 1659–1724, doi:10.1016/S0140-6736(16)31679-8, 2016.

613 Gettelman, A., Liu, X., Barahona, D., Lohmann, U. and Chen, C.: Climate impacts of ice
614 nucleation, *J. Geophys. Res. Atmos.*, 117(20), 1–14, doi:10.1029/2012JD017950, 2012.

615 Ghan, S. J.: Technical note: Estimating aerosol effects on cloud radiative forcing, *Atmos. Chem.*
616 *Phys.*, 13(19), 9971–9974, doi:10.5194/acp-13-9971-2013, 2013.

617 Ghan, S. J., Liu, X., Easter, R. C., Zaveri, R., Rasch, P. J., Yoon, J. H. and Eaton, B.: Toward a
618 minimal representation of aerosols in climate models: Comparative decomposition of aerosol
619 direct, semidirect, and indirect radiative forcing, *J. Clim.*, 25(19), 6461–6476, doi:10.1175/JCLI-
620 D-11-00650.1, 2012.

621 Hanbar, R. D. and Karve, P.: National Programme on Improved Chulha (NPIC) of the
622 Government of India: An overview, *Energy Sustain. Dev.*, 6(2), 49–55, doi:10.1016/S0973-
623 0826(08)60313-0, 2002.

624 He, C., Li, Q. B., Liou, K. N., Zhang, J., Qi, L., Mao, Y., Gao, M., Lu, Z., Streets, D. G., Zhang,
625 Q., Sarin, M. M. and Ram, K.: A global 3-D CTM evaluation of black carbon in the Tibetan
626 Plateau, *Atmos. Chem. Phys.*, 14(13), 7091–7112, doi:10.5194/acp-14-7091-2014, 2014.

627 He, J. and Zhang, Y.: Improvement and further development in CESM/CAM5: Gas-phase
628 chemistry and inorganic aerosol treatments, *Atmos. Chem. Phys.*, 14(17), 9171–9200,
629 doi:10.5194/acp-14-9171-2014, 2014.

630 Holben, B. N., Eck, T. F., Slutsker, I., Tanré, D., Buis, J. P., Setzer, A., Vermote, E., Reagan, J.
631 A., Kaufman, Y. J., Nakajima, T., Lavenu, F., Jankowiak, I. and Smirnov, A.: AERONET—A
632 Federated Instrument Network and Data Archive for Aerosol Characterization, *Remote Sens.*
633 *Environ.*, 66(1), 1–16, doi:10.1016/S0034-4257(98)00031-5, 1998.

634 Holben, B. N., Tanré, D., Smirnov, a., Eck, T. F., Slutsker, I., Abuhassan, N., Newcomb, W. W.,
635 Schafer, J. S., Chatenet, B., Lavenu, F., Kaufman, Y. J., Castle, J. Vande, Setzer, a., Markham,
636 B., Clark, D., Frouin, R., Halthore, R., Karneli, a., O’Neill, N. T., Pietras, C., Pinker, R. T.,
637 Voss, K. and Zibordi, G.: An emerging ground-based aerosol climatology: Aerosol optical depth
638 from AERONET, *J. Geophys. Res.*, 106(D11), 12067, doi:10.1029/2001JD900014, 2001.

639 Huang, Y., Wu, S., Dubey, M. K. and French, N. H. F.: Impact of aging mechanism on model
640 simulated carbonaceous aerosols, *Atmos. Chem. Phys.*, 13(13), 6329–6343, doi:10.5194/acp-13-
641 6329-2013, 2013.

642 Jacobson, M. Z.: Global direct radiative forcing due to multicomponent natural and anthropogenic
643 aerosols, *J. Geophys. Res.*, 106(D2), 1551–1568, doi:10.1029/2000JD900514, 2001a.

644 Jacobson, M. Z.: Strong radiative heating due to the mixing state of black carbon in atmospheric
645 aerosols., *Nature*, 409(6821), 695–697, doi:10.1038/35055518, 2001b.

646 Janssens-Maenhout, G., Crippa, M., Guizzardi, D., Dentener, F., Muntean, M., Pouliot, G.,
647 Keating, T., Zhang, Q., Kurokawa, J., Wankmüller, R., Denier van der Gon, H., Kuenen, J. J. P.,
648 Klimont, Z., Frost, G., Darras, S., Koffi, B. and Li, M.: HTAP_v2.2: a mosaic of regional and
649 global emission grid maps for 2008 and 2010 to study hemispheric transport of air pollution,
650 *Atmos. Chem. Phys.*, 15(19), 11411–11432, doi:10.5194/acp-15-11411-2015, 2015.

651 Kanagawa, M. and Nakata, T.: Analysis of the energy access improvement and its socio-
652 economic impacts in rural areas of developing countries, *Ecol. Econ.*, 62(2), 319–329,
653 doi:10.1016/j.ecolecon.2006.06.005, 2007.

654 Karcher, B. and Hendricks, J.: Physically based parameterization of cirrus cloud formation for
655 use in global atmospheric models, *J. Geophys. Res.*, 111, D01205, doi:10.1029/2005JD006219,
656 2006.

657 Kishore, V. V. N. and Ramana, P. V.: Improved cookstoves in rural India: How improved are
658 they? A critique of the perceived benefits from the National Programme on Improved Chulhas
659 (NPIC), *Energy*, 27(1), 47–63, doi:10.1016/S0360-5442(01)00056-1, 2002.

660 Klimont, Z., Cofala, J., Wei, W., Zhang, C., Wang, S., Kejun, J., Bhandari, P., Mathur, R.,
661 Purohit, P., Rafaj, P., Chambers, A., Amann, M. and Hao, J.: Projections of SO₂, NO_x and
662 carbonaceous aerosols emissions in Asia, *Tellus, Ser. B Chem. Phys. Meteorol.*, (61B), 602–617,
663 doi:10.1111/j.1600-0889.2009.00428.x, 2009.

664 Klimont, Z., Kupiainen, K., Heyes, C., Purohit, P., Cofala, J., Rafaj, P., Borken-Kleefeld, J. and
665 Schöpp, W.: Global anthropogenic emissions of particulate matter including black carbon,

666 Atmos. Chem. Phys., 17(14), 8681–8723, doi:10.5194/acp-17-8681-2017, 2017.

667 Kodros, J. K., Scott, C. E., Farina, S. C., Lee, Y. H., L'Orange, C., Volckens, J. and Pierce, J. R.:
668 Uncertainties in global aerosols and climate effects due to biofuel emissions, Atmos. Chem.
669 Phys., 15(15), 8577–8596, doi:10.5194/acp-15-8577-2015, 2015.

670 Koehler, K. A., DeMott, P. J., Kreidenweis, S. M., Popovicheva, O. B., Petters, M. D., Carrico,
671 C. M., Kireeva, E. D., Khokhlova, T. D. and Shonija, N. K.: Cloud condensation nuclei and ice
672 nucleation activity of hydrophobic and hydrophilic soot particles, Phys. Chem. Chem. Phys.,
673 11(36), 7906–7920, doi:10.1039/b916865f, 2009.

674 Kooperman, G. J., Pritchard, M. S., Ghan, S. J., Wang, M., Somerville, R. C. J. and Russell, L.
675 M.: Constraining the influence of natural variability to improve estimates of global aerosol
676 indirect effects in a nudged version of the Community Atmosphere Model 5, J. Geophys. Res.
677 Atmos., 117(23), 1–16, doi:10.1029/2012JD018588, 2012.

678 Kulkarni, G., China, S., Liu, S., Nandasiri, M., Sharma, N., Wilson, J., Aiken, A. C., Chand, D.,
679 Laskin, A., Mazzoleni, C., Pekour, M., Shilling, J., Shutthanandan, V., Zelenyuk, A. and Zaveri,
680 R. A.: Ice nucleation activity of diesel soot particles at cirrus relevant temperature conditions:
681 Effects of hydration, secondary organics coating, soot morphology, and coagulation, Geophys.
682 Res. Lett., 43(7), 3580–3588, doi:10.1002/2016GL068707, 2016.

683 Lacey, F. and Henze, D.: Global climate impacts of country-level primary carbonaceous aerosol
684 from solid-fuel cookstove emissions, Environ. Res. Lett., 10(11), 114003, doi:10.1088/1748-
685 9326/10/11/114003, 2015.

686 Lacey, F. G., Henze, D. K., Lee, C. J., van Donkelaar, A. and Martin, R. V.: Transient climate
687 and ambient health impacts due to national solid fuel cookstove emissions, Proc. Natl. Acad.
688 Sci., 114(6), 1269–1274, doi:10.1073/pnas.1612430114, 2017.

689 Lamarque, J. F., Emmons, L. K., Hess, P. G., Kinnison, D. E., Tilmes, S., Vitt, F., Heald, C. L.,
690 Holland, E. A., Lauritzen, P. H., Neu, J., Orlando, J. J., Rasch, P. J. and Tyndall, G. K.: CAM-
691 chem: Description and evaluation of interactive atmospheric chemistry in the Community Earth
692 System Model, Geosci. Model Dev., 5(2), 369–411, doi:10.5194/gmd-5-369-2012, 2012.

693 Legros, G., Havet, I., Bruce, N. and Bonjour, S.: The Energy Access Situation in Developing
 694 Countries, WHO UNDP, 142 [online] Available from:
 695 <http://scholar.google.com/scholar?hl=en&btnG=Search&q=intitle:THE+ENERGY+ACCESS+SITUATION+IN+DEVELOPING+COUNTRIES+A+Review+Focusing+on+the#0>, 2009.
 696

697 Lelieveld, J., Evans, J. S., Fnais, M., Giannadaki, D. and Pozzer, A.: The contribution of outdoor
 698 air pollution sources to premature mortality on a global scale, *Nature*, 525(7569), 367–371,
 699 doi:10.1038/nature15371, 2015.

700 Liu, J., Mauzerall, D. L., Chen, Q., Zhang, Q., Song, Y., Peng, W., Klimont, Z., Qiu, X., Zhang,
 701 S., Hu, M., Lin, W., Smith, K. R. and Zhu, T.: Air pollutant emissions from Chinese households:
 702 A major and underappreciated ambient pollution source, *Proc. Natl. Acad. Sci.*, 113(28), 7756–
 703 7761, doi:10.1073/pnas.1604537113, 2016.

704 Liu, X. and Penner, J. E.: Ice nucleation parameterization for global models, *Meteorol.*
 705 *Zeitschrift*, 14(4), 499–514, doi:10.1127/0941-2948/2005/0059, 2005.

706 Liu, X., Penner, J. E., Ghan, S. J. and Wang, M.: Inclusion of ice microphysics in the NCAR
 707 Community Atmospheric Model version 3 (CAM3), *J. Clim.*, 20(18), 4526–4547,
 708 doi:10.1175/JCLI4264.1, 2007.

709 Liu, X., Easter, R. C., Ghan, S. J., Zaveri, R., Rasch, P., Shi, X., Lamarque, J. F., Gettelman, A.,
 710 Morrison, H., Vitt, F., Conley, A., Park, S., Neale, R., Hannay, C., Ekman, A. M. L., Hess, P.,
 711 Mahowald, N., Collins, W., Iacono, M. J., Bretherton, C. S., Flanner, M. G. and Mitchell, D.:
 712 Toward a minimal representation of aerosols in climate models: Description and evaluation in
 713 the Community Atmosphere Model CAM5, *Geosci. Model Dev.*, 5(3), 709–739,
 714 doi:10.5194/gmd-5-709-2012, 2012.

715 Lohmann, U.: A glaciation indirect aerosol effect caused by soot aerosols, *Geophys. Res. Lett.*,
 716 29(4), 1052, doi:10.1029/2001gl014357, 2002.

717 Lohmann, U., Feichter, J., Penner, J. and Leaitch, R.: Indirect effect of sulfate and carbonaceous
 718 aerosols: A mechanistic treatment, *J. Geophys. Res. Atmos.*, 105(D10), 12193–12206,
 719 doi:10.1029/1999JD901199, 2000.

720 Lu, Z., Zhang, Q. and Streets, D. G.: Sulfur dioxide and primary carbonaceous aerosol emissions
 721 in China and India, 1996-2010, *Atmos. Chem. Phys.*, 11(18), 9839–9864, doi:10.5194/acp-11-
 722 9839-2011, 2011.

723 Malm, W. C., Sisler, J. F., Huffman, D., Eldred, R. A. and Cahill, T. A.: Spatial and seasonal
 724 trends in particle concentration and optical extinction in the United States, *J. Geophys. Res.*,
 725 99(D1), 1347–1370, doi:10.1029/93JD02916, 1994.

726 Myhre, G., Samset, B. H., Schulz, M., Balkanski, Y., Bauer, S., Bernsten, T. K., Bian, H.,
 727 Bellouin, N., Chin, M., Diehl, T., Easter, R. C., Feichter, J., Ghan, S. J., Hauglustaine, D.,
 728 Iversen, T., Kinne, S., Kirkevåg, A., Lamarque, J. F., Lin, G., Liu, X., Lund, M. T., Luo, G., Ma,
 729 X., Van Noije, T., Penner, J. E., Rasch, P. J., Ruiz, A., Seland, Skeie, R. B., Stier, P., Takemura,
 730 T., Tsigaridis, K., Wang, P., Wang, Z., Xu, L., Yu, H., Yu, F., Yoon, J. H., Zhang, K., Zhang, H.
 731 and Zhou, C.: Radiative forcing of the direct aerosol effect from AeroCom Phase II simulations,
 732 *Atmos. Chem. Phys.*, 13(4), 1853–1877, doi:10.5194/acp-13-1853-2013, 2013.

733 Pan, X., Chin, M., Gautam, R., Bian, H., Kim, D., Colarco, P. R., Diehl, T. L., Takemura, T. and
 734 Pozzoli, L.: A multi-model evaluation of aerosols over South Asia : common, , 5903–5928,
 735 doi:10.5194/acp-15-5903-2015, 2015.

736 Penner, J. E., Dickinson, R. E. and O'Neill, C. A.: Effects of Aerosol from Biomass Burning on
 737 the Global Radiation Budget, *Science*, 256(5062), 1432–1435,
 738 doi:10.1126/science.256.5062.1432, 1992.

739 Penner, J. E., Chen, Y., Wang, M. and Liu, X.: Possible influence of anthropogenic aerosols on
 740 cirrus clouds and anthropogenic forcing, *Atmos. Chem. Phys.*, 9(3), 879–896, doi:10.5194/acp-9-
 741 879-2009, 2009.

742 Pierce, J. R., Chen, K. and Adams, P. J.: Contribution of carbonaceous aerosol to cloud
 743 condensation nuclei: processes and uncertainties evaluated with a global aerosol microphysics
 744 model, *Atmos. Chem. Phys.*, 7, 5447–5466, doi:10.5194/acp-7-5447-2007, 2007.

745 Quennehen, B., Raut, J. C., Law, K. S., Daskalakis, N., Ancellet, G., Clerbaux, C., Kim, S. W.,
 746 Lund, M. T., Myhre, G., Olivié, D. J. L., Safieddine, S., Skeie, R. B., Thomas, J. L., Tsyro, S.,

747 Bazureau, A., Bellouin, N., Hu, M., Kanakidou, M., Klimont, Z., Kupiainen, K.,
 748 Myriokefalitakis, S., Quaas, J., Rumbold, S. T., Schulz, M., Cherian, R., Shimizu, A., Wang, J.,
 749 Yoon, S. C. and Zhu, T.: Multi-model evaluation of short-lived pollutant distributions over east
 750 Asia during summer 2008, *Atmos. Chem. Phys.*, 16(17), 10765–10792, doi:10.5194/acp-16-
 751 10765-2016, 2016.

752 Reddington, C. L., Spracklen, D. V., Artaxo, P., Ridley, D. A., Rizzo, L. V. and Arana, A.:
 753 Analysis of particulate emissions from tropical biomass burning using a global aerosol model
 754 and long-term surface observations, *Atmos. Chem. Phys.*, 16(17), 11083–11106,
 755 doi:10.5194/acp-16-11083-2016, 2016.

756 Riahi, K., Rao, S., Krey, V., Cho, C., Chirkov, V., Fischer, G., Kindermann, G., Nakicenovic, N.
 757 and Rafaj, P.: RCP 8.5-A scenario of comparatively high greenhouse gas emissions, *Clim.*
 758 *Change*, 109(1), 33–57, doi:10.1007/s10584-011-0149-y, 2011.

759 Schulz, M., Textor, C., Kinne, S., Balkanski, Y., Bauer, S., Bernsten, T., Berglen, T., Boucher,
 760 O., Dentener, F., Guibert, S., Isaksen, I. S. a., Iversen, T., Koch, D., Kirkevåg, A., Liu, X.,
 761 Montanaro, V., Myhre, G., Penner, J. E., Pitari, G., Reddy, S., Seland, Ø., Stier, P. and
 762 Takemura, T.: Radiative forcing by aerosols as derived from the AeroCom present-day and pre-
 763 industrial simulations, *Atmos. Chem. Phys.*, 6, 5225–5246, doi:10.5194/acpd-6-5095-2006,
 764 2006.

765 Smith, K. R., Bruce, N., Balakrishnan, K., Adair-Rohani, H., Balmes, J., Chafe, Z., Dherani, M.,
 766 Hosgood, H. D., Mehta, S., Pope, D. and Rehfuess, E.: Millions Dead: How Do We Know and
 767 What Does It Mean? Methods Used in the Comparative Risk Assessment of Household Air
 768 Pollution, *Annu. Rev. Public Health*, 35(1), 185–206, doi:10.1146/annurev-publhealth-032013-
 769 182356, 2014.

770 Spracklen, D. V., Jimenez, J. L., Carslaw, K. S., Worsnop, D. R., Evans, M. J., Mann, G. W.,
 771 Zhang, Q., Canagaratna, M. R., Allan, J., Coe, H., McFiggans, G., Rap, A. and Forster, P.:
 772 Aerosol mass spectrometer constraint on the global secondary organic aerosol budget, *Atmos.*
 773 *Chem. Phys.*, 11(23), 12109–12136, doi:10.5194/acp-11-12109-2011, 2011a.

774 Spracklen, D. V., Carslaw, K. S., Pöschl, U., Rap, A. and Forster, P. M.: Global cloud

condensation nuclei influenced by carbonaceous combustion aerosol, *Atmos. Chem. Phys.*,
11(17), 9067–9087, doi:10.5194/acp-11-9067-2011, 2011b.

Stohl, A., Aamaas, B., Amann, M., Baker, L. H., Bellouin, N., Berntsen, T. K., Boucher, O.,
Cherian, R., Collins, W., Daskalakis, N., Dusinska, M., Eckhardt, S., Fuglestad, J. S., Harju,
M., Heyes, C., Hodnebrog, Hao, J., Im, U., Kanakidou, M., Klimont, Z., Kupiainen, K., Law, K.
S., Lund, M. T., Maas, R., MacIntosh, C. R., Myhre, G., Myriokefalitakis, S., Olivie, D., Quaas,
J., Quennehen, B., Raut, J. C., Rumbold, S. T., Samset, B. H., Schulz, M., Seland, Shine, K. P.,
Skeie, R. B., Wang, S., Yttri, K. E. and Zhu, T.: Evaluating the climate and air quality impacts of
short-lived pollutants, *Atmos. Chem. Phys.*, 15(18), 10529–10566, doi:10.5194/acp-15-10529-
2015, 2015.

Streets, D. G., Yan, F., Chin, M., Diehl, T., Mahowald, N., Schultz, M., Wild, M., Wu, Y. and
Yu, C.: Anthropogenic and natural contributions to regional trends in aerosol optical depth,
1980–2006, *J. Geophys. Res. Atmos.*, 114(14), 1–16, doi:10.1029/2008JD011624, 2009.

Textor, C., Schulz, M., Guibert, S., Kinne, S., Balkanski, Y., Bauer, S., Berntsen, T., Berglen, T.,
Boucher, O., Chin, M., Dentener, F., Diehl, T., Easter, R., Feichter, H., Fillmore, D., Ghan, S.,
Ginoux, P., Gong, S., Grini, A., Hendricks, J., Horowitz, L., Huang, P., Isaksen, I., Iversen, I.,
Kloster, S., Koch, D., Kirkevåg, A., Kristjansson, J. E., Krol, M., Lauer, A., Lamarque, J. F., Liu,
X., Montanaro, V., Myhre, G., Penner, J., Pitari, G., Reddy, S., Seland, Ø., Stier, P., Takemura,
T. and Tie, X.: Analysis and quantification of the diversities of aerosol life cycles within
AeroCom, *Atmos. Chem. Phys.*, 6(7), 1777–1813, doi:10.5194/acp-6-1777-2006, 2006.

Tilmes, S., Lamarque, J. F., Emmons, L. K., Kinnison, D. E., Ma, P. L., Liu, X., Ghan, S.,
Bardeen, C., Arnold, S., Deeter, M., Vitt, F., Ryerson, T., Elkins, J. W., Moore, F., Spackman, J.
R. and Val Martin, M.: Description and evaluation of tropospheric chemistry and aerosols in the
Community Earth System Model (CESM1.2), *Geosci. Model Dev.*, 8(5), 1395–1426,
doi:10.5194/gmd-8-1395-2015, 2015.

Venkataraman, C., Habib, G., Eiguren-Fernandez, A., Miguel, A. H. and Friendlander, S. K.:
Residential Biofuels in South Asia: Carbonaceous Aerosol Emissions and Climate Impacts,
Science, 307(5714), 1454–1456, doi:10.1126/science.1104359, 2005.

803 Venkataraman, C., Sagar, A. D., Habib, G., Lam, N. and Smith, K. R.: The Indian National
804 Initiative for Advanced Biomass Cookstoves: The benefits of clean combustion, *Energy Sustain.*
805 *Dev.*, 14(2), 63–72, doi:10.1016/j.esd.2010.04.005, 2010.

806 Wang, Q., Jacob, D. J., Fisher, J. A., Mao, J., Leibensperger, E. M., Carouge, C. C., Le Sager, P.,
807 Kondo, Y., Jimenez, J. L., Cubison, M. J. and Doherty, S. J.: Sources of carbonaceous aerosols
808 and deposited black carbon in the Arctic in winter-spring: Implications for radiative forcing,
809 *Atmos. Chem. Phys.*, 11(23), 12453–12473, doi:10.5194/acp-11-12453-2011, 2011.

810 Wang, Q., Jacob, D. J., Spackman, J. R., Perring, A. E., Schwarz, J. P., Moteki, N., Marais, E.
811 A., Ge, C., Wang, J. and Barrett, S. R. H.: Global budget and radiative forcing of black carbon
812 aerosol: Constraints from pole-to-pole (HIPPO) observations across the Pacific, *J. Geophys.*
813 *Res.*, 119(1), 195–206, doi:10.1002/2013JD020824, 2014a.

814 Wang, X., Heald, C. L., Ridley, D. A., Schwarz, J. P., Spackman, J. R., Perring, A. E., Coe, H.,
815 Liu, D. and Clarke, A. D.: Exploiting simultaneous observational constraints on mass and
816 absorption to estimate the global direct radiative forcing of black carbon and brown carbon,
817 *Atmos. Chem. Phys.*, 14(20), 10989–11010, doi:10.5194/acp-14-10989-2014, 2014b.

818 Ward, D. S., Kloster, S., Mahowald, N. M., Rogers, B. M., Randerson, J. T. and Hess, P. G.: The
819 changing radiative forcing of fires: global model estimates for past, present and future, *Atmos.*
820 *Chem. Phys.*, 12, 10857–10886, doi:10.5194/acp-12-10857-2012, 2012.

821 Zhang, L., Henze, D. K., Grell, G. A., Carmichael, G. R., Bousserez, N., Zhang, Q., Torres, O.,
822 Ahn, C., Lu, Z., Cao, J. and Mao, Y.: Constraining black carbon aerosol over Asia using OMI
823 aerosol absorption optical depth and the adjoint of GEOS-Chem, *Atmos. Chem. Phys.*, 15(18),
824 10281–10308, doi:10.5194/acp-15-10281-2015, 2015.

825 Zhang, Q., Jimenez, J. L., Canagaratna, M. R., Allan, J. D., Coe, H., Ulbrich, I., Alfarra, M. R.,
826 Takami, A., Middlebrook, A. M., Sun, Y. L., Dzepina, K., Dunlea, E., Docherty, K., DeCarlo, P.
827 F., Salcedo, D., Onasch, T., Jayne, J. T., Miyoshi, T., Shimojo, A., Hatakeyama, S., Takegawa,
828 N., Kondo, Y., Schneider, J., Drewnick, F., Borrmann, S., Weimer, S., Demerjian, K., Williams,
829 P., Bower, K., Bahreini, R., Cottrell, L., Griffin, R. J., Rautiainen, J., Sun, J. Y., Zhang, Y. M.
830 and Worsnop, D. R.: Ubiquity and dominance of oxygenated species in organic aerosols in

831 anthropogenically-influenced Northern Hemisphere midlatitudes, *Geophys. Res. Lett.*, 34(13), 1–
832 6, doi:10.1029/2007GL029979, 2007.

833 Zheng, Y., Unger, N., Hodzic, A., Emmons, L., Knote, C., Tilmes, S., Lamarque, J. F. and Yu,
834 P.: Limited effect of anthropogenic nitrogen oxides on Secondary Organic Aerosol formation,
835 *Atmos. Chem. Phys.*, 15(23), 23231–23277, doi:10.5194/acpd-15-23231-2015, 2015.

836

837

838

839

840

841

842

843

844

845

846

847

848

849

850

851

852 **Table 1. Annual budget for various species for the BASE, GBLSF_OFF and INDSF_OFF**
853 **simulations for the year 2010.**

Specie	ECLIPSE V5a (BASE) ^a	GBLSF_OFF ^a	INDSF_OFF ^a
BC	7.23	4.92	6.87
POM	18.9	8.53	17.2
SO ₂	98.5	97.1	98.37
NO _x	120.5	118	119.8
VOC	81.1	52.4	76.6
CO	548	358	516
NH ₃	54.9	54.6	54.87

854 ^aUnits are Tg specie/yr.

855

856

857

858

859

860

861

862

863

864

865 **Table 2. Model experiments setup.**

Experiments	Anthropogenic emission scenario
BASE	ECLIPSE V5a
GBLSF_OFF	ECLIPSE V5a excluding global solid fuel cookstove emissions
INDSF_OFF	ECLIPSE V5a excluding Indian solid fuel cookstove emissions

866

867

868

869

870

871

872

873

874

875

876

877

878

879

880 **Table 3. Global budgets, burden and lifetime of BC and POM from model control**
 881 **simulations.**

Specie	BC	POM
Sources (Tg specie/yr)	9.73	49.9
fossil fuel and biofuel	7.23	18.9
biomass burning emissions	2.5	31
Sinks (Tg specie/yr)	9.72	49.8
Dry Deposition	1.8	8.14
Wet Deposition	7.92	41.7
Burden (Tg) ^a	0.12 ± 0.001	0.66 ± 0.006
Lifetime (days) ^a	4.5 ± 0.04	4.8 ± 0.04

882 ^astandard deviation represents the uncertainty error owing to temporal variability in the
 883 model.

884

885

886

887

888

889

890

891

892

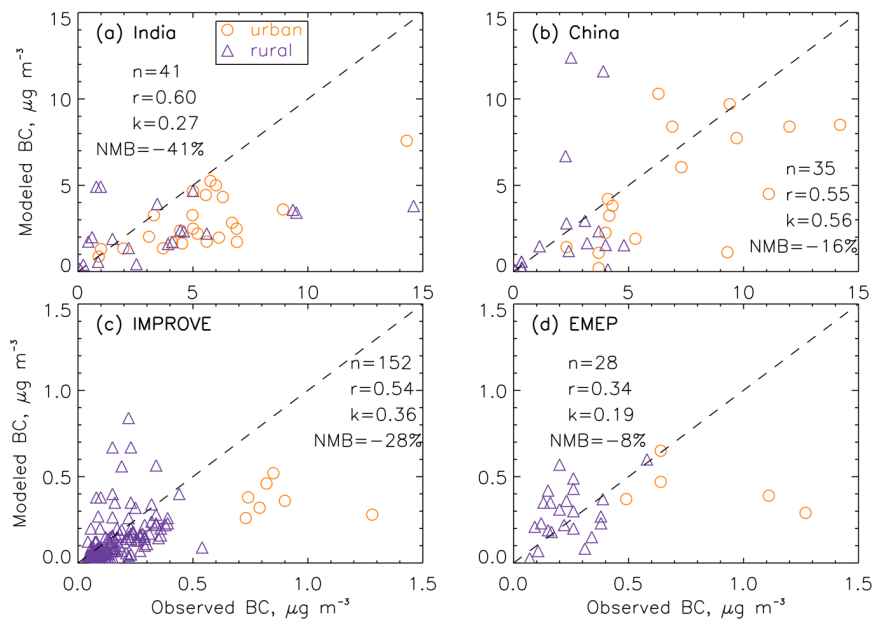
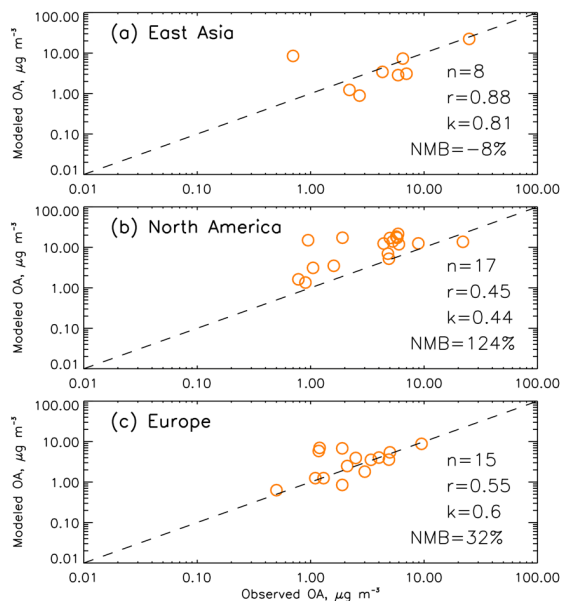


Figure 1. Comparisons of observational and model simulated annual mean surface BC concentrations from (a) India, (b) China, (3) IMPROVE, and (d) EMEP. Urban and rural sites are shown in orange circles and blue triangles for each region. For each panel, the total number of observational sites (n), model-to-observation regression slopes (k), correlation coefficient (r) and NMB values are included. The dashed line in each panel represents the 1:1 ratio.

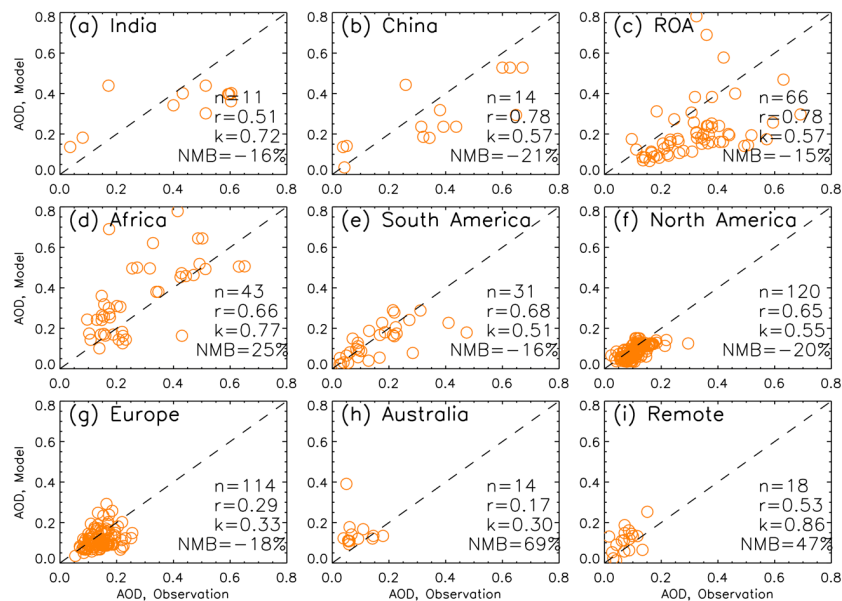


902

903 **Figure 2.** Comparisons of observational and model simulated surface OA concentrations from (a)
 904 East Asia, (b) North America, and (3) Europe. For each panel, the total number of observational
 905 sites (n), model-to-observation regression slopes (k), correlation coefficient (r) and NMB values
 906 are included. The dashed line in each panel represents the 1:1 ratio.

907

908



909

910 **Figure 3.** Scatter plots of AOD between model simulation and observations over (a) India, (b)
 911 China, (c) Rest of Asia (ROA), excluding China and India, (d) Africa, (e) South America, (f) North
 912 America, (g) Europe, (h) Australia and (i) Remote. For each panel, the total number of
 913 observational sites (n), model-to-observation regression slopes (k), correlation coefficient (r) and
 914 NMB are included.

915

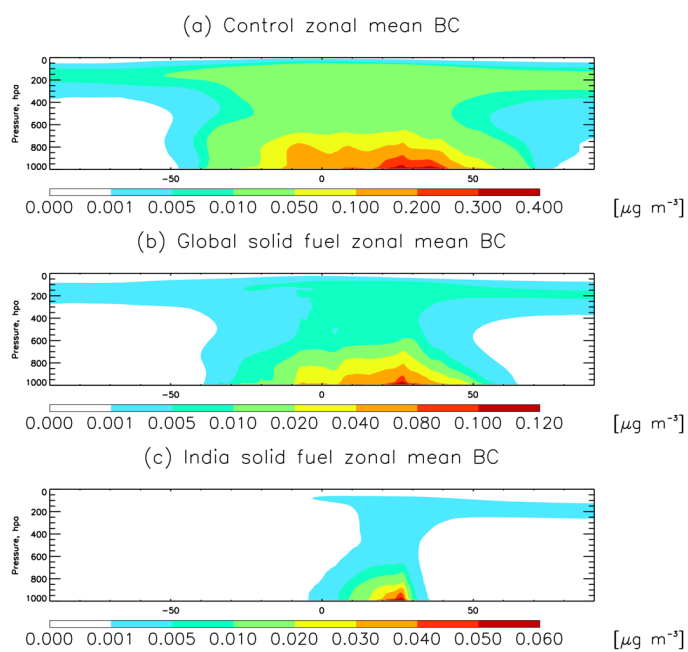


Figure 4. Annual zonal mean BC concentrations from (a) the BASE simulation, (b) the global and (c) India solid fuel cookstove emissions. BC concentrations are calculated under standard temperature and pressure conditions (273 K, 1 atm).

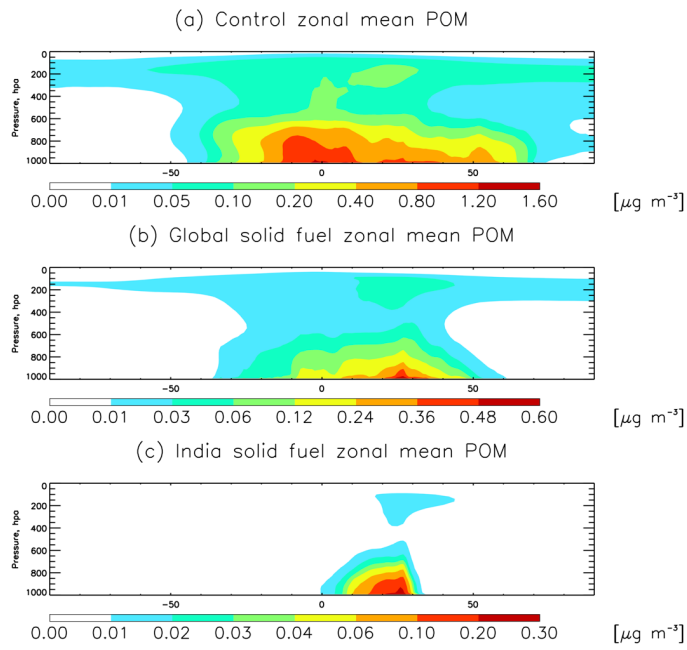


Figure 5. Same as Fig. 4 but for POM.

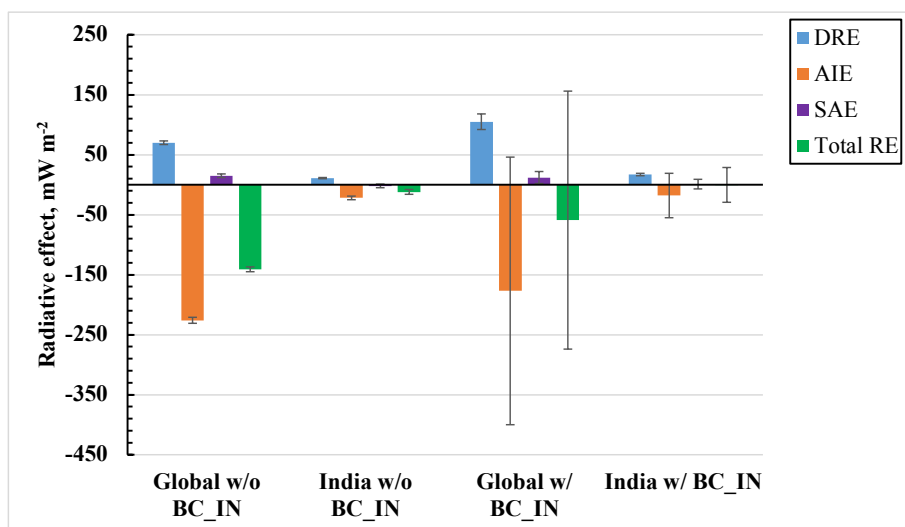


Figure 6. Radiative effect (RE) for global and Indian solid fuel cookstove aerosol emissions with BC not serving as IN (w/o BC_IN) and BC as IN (BC_IN), with DRE (blue), AIE (orange), SAE (purple) and total RE (green). Error bars represent one standard deviation for each RE. For BC as IN, standard deviations of RE are solely based on the choices of maximum freezing efficiency of BC as 0.01, 0.05 and 0.1 respectively.

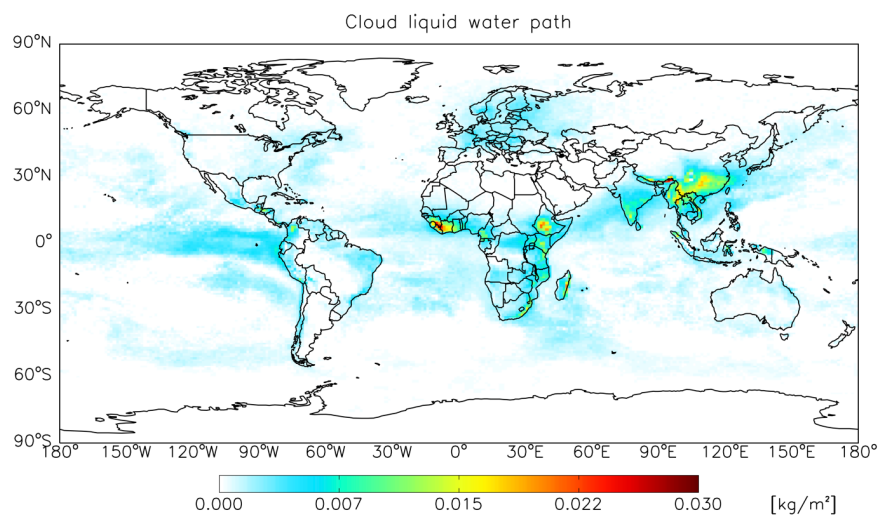


Figure 7. Global vertically-integrated cloud liquid water path from the global solid fuel cookstove emissions.

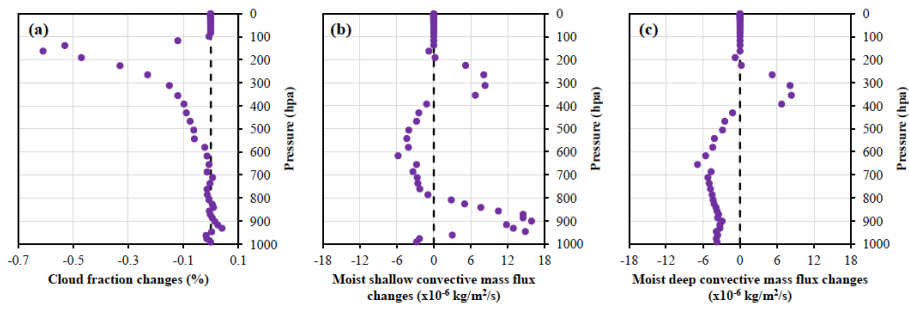


Figure 8. Changes in vertical cloud fractions (a), shallow (b) and deep (c) convective mass flux within the India and Indian Ocean domain from global solid fuel cookstove emissions.

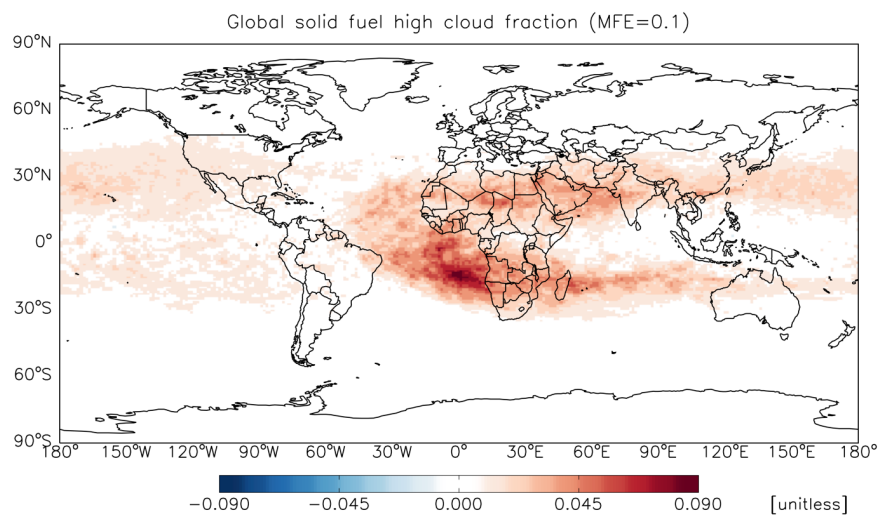


Figure 9. Global distribution of high cloud fraction due to solid fuel cookstove aerosol emissions with BC as IN and MFE=0.1.

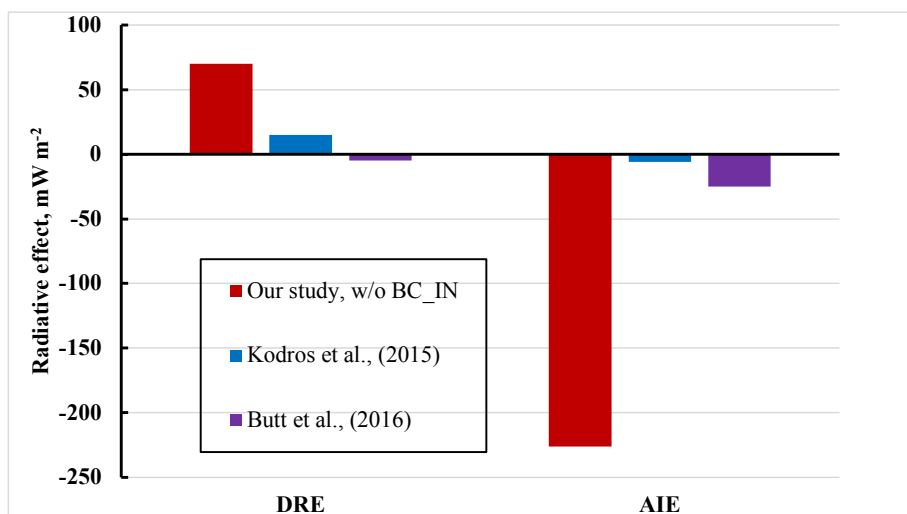


Figure 10. Comparisons of DRE (left) and AIE (right) radiative effects from global solid fuel cookstove emissions in our control simulation with Kodros et al. (2015) and Butt et al. (2016).